SIMULATION OF SOLID-LIQUID FLOW IN STIRRED TANKS AT HIGH SOLID LOADING

Divyamaan WADNERKAR, Ranjeet P. UTIKAR*, Moses O. TADE, Vishnu K. PAREEK

Department of Chemical Engineering, Curtin University, Perth, WA 6102
*Corresponding author, E-mail address: r.utikar@curtin.edu.au

ABSTRACT

Solid liquid stirred tanks are commonly used in mineral industry for operations like concentration, leaching, adsorption, effluent treatment, etc. Hydrodynamic study is necessary to evaluate the performance of such systems. Especially, in the cases of high solid concentration, the flow field, slip velocity, turbulence and drag are significantly different from the single phase values and therefore, such studies become indispensable. In this study, the change in these parameters in the presence of solids and the effect of high solid concentration is discussed. Eulerian-eulerian multiphase modelling approach was used to simulate the solid suspension in stirred tanks. Multiple reference frame (MRF) approach was used to simulate the impeller rotation in a fully baffled tank. Simulations were conducted using commercial CFD solver ANSYS Fluent 13.0. The CFD simulations were conducted for concentration 20 wt% and the impeller speeds at the just suspension speed. The solid-liquid interaction was taken into account using modified Brucato drag model. A substantial decrease in the flow number was observed due to the presence of solids. The dampening of turbulence was evident in the impeller region where the solid concentration was the maximum. The drag was able to account the increase in drag at high turbulent intensities. The predictions in terms of the velocity profiles were found to be in reasonable agreement with the experimental data of Guida et al. (2010). The work provides an insight into the solid liquid flow in stirred tanks with high solid concentration and will be useful for applications such as carbon in leach circuit which operates at high solid loading.

NOMENCLATURE

B_l blade length
B_w blade width
C impeller clearance
C_D drag coefficient
C_{Do} particle drag coefficient in still fluid
D diffusivities
D_i impeller diameter
D_s shaft diameter
d_P particle diameter
$\vec{F}_{td}$ force due to turbulent dissipation
$\vec{F}_q$ external force
$\vec{F}_{lift}$ lift force
$\vec{F}_{vm}$ virtual mass force
$\vec{F}_{12}$ interphase interaction force
g gravity
G_k turbulence kinetic energy
H tank height
$\bar{\bar{I}}$ unit stress tensor.

k turbulence kinetic energy
l continuous phase
m mixture properties
M torque
N impeller speed
N_{js} speed of just suspension
N_{Re} Reynolds number
p pressure and is shared by both the phases
P power delivered to the fluid
q 1 or 2 for primary or secondary phase respectively
Re_p particle Reynolds number
s dispersed phase
T   tank diameter
$\vec{u}$ velocity vector
$\vec{u}_{dr}$ drift velocity
W baffle width
X weight percent

Greek Letters
α volume fraction
ε turbulence dissipation rate
λ Kolmogorov length scale
μ shear viscosity
μ_t turbulent viscosity
ρ density
σ Prandtl numbers
σ_{sl} dispersion Prandtl number
$\bar{\bar{\tau}}$ stress tensor because of viscosity and velocity fluctuations
υ bulk viscosity

INTRODUCTION

High concentration solid-liquid stirred tanks are widely operated in mineral, pharmaceutical, food, paper and pulp industries. Poor mixing in such systems is a common problem. This problem can be solved by increasing the power of impeller and changing the geometrical parameters such as modifying the tank bottom, changing impeller to tank diameter, decreasing clearance, selecting impeller type, altering impeller width, installing baffles, etc.. Merely increasing the impeller speed results in only marginal increase in homogeneity with additional power consumption. Therefore, changing the design parameters is preffered optionwhich still remainsopen problem for design engineers (Guida et al., 2010). In order to make such changes, understanding thehydrodynamics of solid-liquid flow for high solid loading systems is critical. In this paper Eulerian-Eulerian CFD simulations are used to evaluate the performance and flow field distribution with the increase in solid concentration.

Numerous studies are available in literature that discusses the hydrodynamics of solid liquid stirred systems(Kasat et al., 2008; Rasteiro et al., 1994; Sardeshpande, Madhavi V. et al., 2009; Yamazaki et al., 1986). Most of these studies

were conducted on low solid loading stirred tanks. One of the reasons is the lack of tools and techniques that could measure the data with high spatial and temporal resolution at high solid loading. The visual method can only provide qualitative measurement of just suspension speed and cloud height and is only applicable for low solid volume fractions (Sardeshpande, Madhavi V. et al., 2009). Direct sampling affects the withdrawal velocity, geometry configuration and position making measurement inaccurate. Similarly, conductivity probes are invasive as well (Yamazaki et al., 1986). The applicability of flow field measurement based on optical measurement such as light scattering technique (LST), laser Doppler velocimetry (LDV) and particle image velocimetry (PIV) is limited to low concentration due to their inapplicability in high solids loading systems (Pianko-Oprych et al., 2009; Unadkat et al., 2009). The continuous improvements in non-invasive electrical, magnetic and radioactive techniques has made the study of high solid loading stirred tank possible(Barigou, 2004; Guida et al., 2010; Stevenson et al., 2010). The scope of the studies conducted were applicability of these techniques for flow, concentration measurement, investigation of off-bottom suspension and the effect of particle size and concentration on it and generation of data set.However, none of thestudies mentioned above discusses the turbulence level distribution (responsible for the particle suspension) for high solid loading stirred tanks stirred with axial impellers.

Computational modelling has always been presented as an option for the hydrodynamic analysis of such systems as it is far inexpensive and enables the study of detailed description of multiphase flow. CFD modelling, however, can only be applied after proper validation. With the availability of experimental data, researchers have started employing CFD modelsto simulate high solid loading suspension in stirred tanks (Fradette et al., 2007; Ochieng & Lewis, 2006; Rasteiro et al., 1994). In an attempt to find a suitable computation technique for the hydrodynamics simulations, Fradette et al. (2007) assessed the accuracy of Shear-Induced Migration Model (SIMM) to capture the particle suspending phenomenon and particle migration in solid-liquid. Errors were found in large-gap geometries because of large magnitude and opposite signs of shear rate and viscosity terms leading to large discrepancies with respect to the experimental flow and concentration fields.Rasteiro et al. (1994) examined the solid concentration profiles using the sedimentation-dispersion model. They studied the axial variation in concentration with the change in the average concentration, particle size and impeller clearance. Ochieng and Lewis (2006) employed Computational Fluid Dynamics (CFD) to investigate the nickel solids off-bottom suspension and cloud height in a fully baffled elliptical bottomed tank agitated by a hydrofoil propeller Mixtec HA735. In the CFD simulations, they used Gidaspow drag model. In another study, Ochieng and Onyango (Ochieng & Onyango, 2008), assessed different drag models for the simulation of solids in stirred tanks and found that in Stokes law region Gidaspow model provides better results than the Brucato model applicable that provided best prediction in turbulent regimes. They provided a brief overview of variation of slip velocity with particle size and effect of drag models on solids concentration distribution.

While these CFD simulations provide valuable insight into the mixing processes, adequate information key details such as the scale of turbulence energy, dissipation rateand slip velocity distribution in tank is missing high loading systems. This information isuseful for evaluation of mixing efficiency of an impellerthrough simulationsat high concentration of solids. Therefore, a Eulerian-based multiphase simulation isused to investigate the effect of high solid loading on the hydrodynamics of a stirred tank in this paper. The CFD simulation results were initially compared with the experimental velocity field data (Guida et al., 2010) for both the phases. In the later part of the paper, the change in the drag, flow field, velocity components, slip velocity and turbulence kinetic energy are used for evaluating the performance and flow field distribution with the increase in solid concentration are discussed in detail.

MODEL DESCRIPTION

Continuity Equations

The hydrodynamic study is simulated using Eulerian-Eulerian multiphase model. Each phase, in this model, is treated as an interpenetrating continuum represented by a volume fraction at each point of the system. The Reynolds averaged mass and momentum balance equations are solved for each of the phases. The governing equations are given below:

Continuity equation:

$$\frac{\partial}{\partial t}\left(\alpha_q \rho_q\right) + \nabla.\left(\alpha_q \rho_q \vec{u}_q\right) = 0$$

Momentum equation:

$$\frac{\partial}{\partial t}\left(\alpha_q \rho_q \vec{u}_q\right) + \nabla.\left(\alpha_q \rho_q \vec{u}_q \vec{u}_q\right)$$
$$= -\alpha_q \nabla p + \nabla.\overline{\overline{\tau}}_q + \alpha_q \rho_q \vec{g} + \vec{F}_{td}$$
$$+ \vec{F}_q + \vec{F}_{lift,q} + \vec{F}_{vm,q} + \vec{F}_{12}$$

The stress-strain tensor is due to viscosity and Reynolds stresses that include the effect of turbulent fluctuations. Using the Boussinesq's eddy viscosity hypothesis the closure can be given to the above momentum transfer equation. The equation can be given as:

$$\overline{\overline{\tau}}_q = \alpha_q \mu_q \left(\nabla \vec{u}_q + \nabla \vec{u}_q^T\right) + \alpha_q \left(\upsilon_q - \frac{2}{3}\mu_q\right)\nabla \vec{u}_q \overline{\overline{I}}$$

Equations for turbulence

Three models of turbulence can be used for the simulations. The mixture turbulence model assumes the domain as a mixture and solves for k and ε values which are common for both the phases. In the dispersed turbulence model, the modified k-ε equations are solved for the continuous phase and the turbulence quantities of dispersed phase are calculated using Tchen-theory correlations. It also takes the fluctuations due to turbulence by solving for the interphase turbulent momentum transfer. Motante and Magelli (Montante & Magelli, 2005) performed analysis of the turbulence models and found that dispersed turbulence model provided unrealistic results while there was negligible difference in the results between per phase and mixture turbulence model. On this basis, k-ε mixture turbulence is used in the present study.For the sake of brevity, only the equations of mixture model for turbulence are given below. Other equations can be found in the Fluent user guide (ANSYS, 2009).

$$\frac{\partial}{\partial t}(\rho_m k) + \nabla.(\rho_m \vec{u}_m k) = \nabla.\left(\frac{\mu_{t,m}}{\sigma_k}\nabla k\right) + G_{k,m} - \rho_m \varepsilon$$

$$\frac{\partial}{\partial t}(\rho_m \varepsilon) + \nabla.(\rho_m \vec{u}_m \varepsilon) = \nabla.\left(\frac{\mu_{t,m}}{\sigma_\varepsilon}\nabla \varepsilon\right) + \frac{\varepsilon}{k}\left(C_{1\varepsilon}G_{k,m} - C_{2\varepsilon}\rho_m \varepsilon\right)$$

where $C_{1\varepsilon}$ and $C_{2\varepsilon}$ are constants.

$$\rho_m = \sum_{i=1}^{N}\alpha_i \rho_i$$

$$\vec{u}_m = \sum_{i=1}^{N}\alpha_i \rho_i \vec{u}_i \Big/ \sum_{i=1}^{N}\alpha_i \rho_i$$

$$\mu_{t,m} = \rho_m C_\mu \frac{k^2}{\varepsilon}$$

$$G_{k,m} = \mu_{t,m}\left(\vec{\nabla u}_m + \vec{\nabla u}_m^{T}\right):\vec{\nabla u}_m$$

Turbulent dispersion force

Turbulent fluctuations result in dispersion of phases from high volume fraction regions to low volume fraction regions due to turbulent dispersion forces. The significance of turbulence dispersion force is highlighted in some previous studies (Ljungqvist & Rasmuson, 2001). In the simulation of solid suspension in stirred tanks, the turbulent dispersion force is significant when the size of turbulence eddies is larger than the particle size (Kasat et al., 2008).In the simulations, the magnitude of turbulence eddies was found to be of an order higher than the particle diameter. Therefore, turbulent dispersion force was incorporated in the momentum equation and is given as follows:

$$\vec{F}_{t,d} = K_{sl}\vec{u}_{dr}$$

$$\vec{u}_{dr} = -\left(\frac{D_s}{\sigma_{sl}\alpha_s}\nabla\alpha_s - \frac{D_l}{\sigma_{sl}\alpha_l}\nabla\alpha_l\right)$$

where, s is dispersed phase and l is continuous phase, D_s and D_l are diffusivities and σ_{sl} is dispersion Prandtl number.

Interphase drag force

Interphase drag is the resultant force experienced by the particle in the direction of relative motion due to relative motion to a fluid. Since, the solid-liquid are treated as interpenetrating phase in Eulerian-Eulerian modelling, an inter-phase momentum exchange term is used, which is given as

$$\vec{F}_{12} = \frac{3}{4}C_D\frac{\alpha_s\alpha_l\rho_l|\vec{v}_s - \vec{v}_l|^2}{d_p}$$

Different correlations are available for calculating interphase drag coefficient viz. Gidaspow, Wen and Yu, Brucato and modified Brucato Drag models (Wadnerkar et al., 2012). For the turbulent flow in stirred tank, Wadnerkar et al. (2012) conducted simulations and assessed these four drag models. They found modified Brucato as the most appropriate for such cases. On their recommendation, modified Brucato drag model was used in the simulations. The modified Brucato drag model is given as:

$$\left(\frac{C_D - C_{Do}}{C_{Do}}\right) = K\left(\frac{d_p}{\lambda}\right)^3$$

where, K is constant with value 8.76×10^{-5}.
C_{Do} is given as

$$C_{Do} = \frac{24}{\alpha_l N_{Re}}\left[1 + 0.15(\alpha_l N_{Re})^{0.687}\right]$$

METHODOLOGY AND BOUNDARY CONDITIONS

Vessel geometry

Tank (in m)		PBT (in m)		Material	
T	0.288	D	0.144	ρ_l	$1150 kg/m^3$
H	0.288	B_l	0.055	ρ_p	$2585 kg/m^3$
W	0.0288	B_w	0.041	d_p	0.003 m
C	0.072	D_{shaft}	0.01	X	0-50 wt%

Table 1: Dimensions of domain and properties of materials used in this study.

In the current study, a flat bottomed cylindrical tank was simulated (see Figure 1). The shaft of the impeller was concentric with the axis of the tank.A 45°six-bladed Pitched Blade Turbine (PBT) was used as an impeller.The dimensions of tank and impeller are given in Table 1. The fluid and particle properties used in the simulation are also tabulated in the same table.
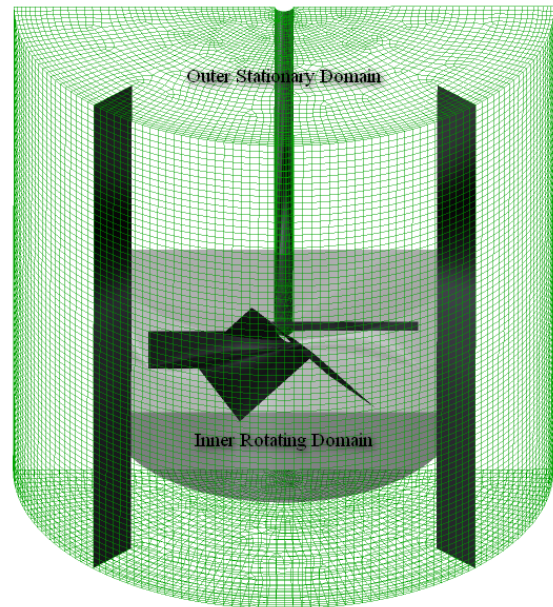
Figure 1: Computational domain and grid distribution in stirred tank

Numerical simulations

Owing to the rotationally periodic nature, half of the tank was simulated. Multiple reference frame (MRF) approach was used. A reference moving zone with dimensions r = 0.06 m and 0.036< z < 0.137 was created (where z is the axial distance from the bottom). The impeller rod outside this zone was considered as a moving wall. Impellers used in all the cases simulated in the study were operated in the down-pumping mode. The top of the tank was open, so it was defined as a wall of zero shear.In the initial condition of the simulation, a uniform average concentration of particles was taken in the tank. The speed of just suspension, N_{js}, was used as the rotation speed of the impeller. For modelling the turbulence, a standard k- ε mixture model was used. The model parameters were Cμ : 0.09, C_1 : 1.44, C_2 : 1.92, σ_k: 1.0 and σ_ε = 1.3. The transient numerical solution of the system was obtained by using the commercial CFD solver ANSYS 13.1 FLUENT. In the present work, SIMPLE scheme was used forPressure-Velocity coupling along with the standard

pressure discretization scheme. The grid independency of the geometry was checked by conducting single phase flow simulations on total number computational grid of 275036,400246 and 648430 cells. The prediction of power number predicted by grid of 275036,400246 and 648430 cells was 1.95, 1.69 and 1.67 respectively. Therefore, no any considerable change in the power number for the grid of 400246 cells was observed with further grid refinement and it was used for the cases simulated for the study. The details of cases simulated and discussed in the chapter are given in Table 2.

The convergence of the simulation was verified by monitoring residual values as well as additional parameters namely turbulence dissipation over the volume, turbulence dissipation at the surface right below impeller and torque on the shaft. Once the residuals and additional parameters were constant, a simulation was deemed to be converged. The simulations were conducted for 10 s with a time step of 0.0001 s. The time averaged data for last 2.5 s was used for the comparison of results.

C (wt %)	N_{js} (RPM)	N_{Re} ($\times 10^5$)
0	330	1.31
20	480	1.91
40	590	2.34

Table 2: Details of cases simulated

RESULTS AND DISCUSSION

The drag model used in the paper has been tested for systems with particle Reynolds number upto 2857 (Khopkar et al., 2006). The cases studied in this paper are simulated for particle Reynolds number higher than that. Therefore, an investigation was conducted to ensure the validity of the model for the cases studied in the paper. The dimensions and properties of vessel and materials respectively are kept similar to the paper of Guida et al. (2010) for the ease of validation. The validated cases were used for the further analysis of flow field, slip velocity, turbulence kinetic energy and turbulent dissipation in the tank.

Validation of Drag model

Wadnerkar et al. (2012) showed that for low solid holdups the modified Brucato drag model performs better compared to the other drag models. To assess the applicability at higher particle Reynolds number, initial simulations were conducted using this drag model and the results were compared with the axial, radial and tangential velocity components for the same set of conditions as are available in literature (Guida et al., 2010). The spatial resolution of PEPT technology depends on the particle velocity (Chaouki et al., 1997). From the maximum particle velocity magnitude from the experiments, the resolution was found to be 4 mm. Considering this limitation, the CFD results are reported on ensemble average basis in a 4 mm zone around the centreline of the measurement point.

The comparison of radial, axial and tangential velocities of solid particles at impeller discharge plane are shown in figure 2 for the case of 20wt% solids. From the plot, the applicability of the drag model for this case is evident. The model is successfully able to predict the three velocity components quantitatively. However, there is a mismatch in the location of peak value of maximum downward axial velocity. The peak in the simulation has shifted radially outwards. This is because of the change in angle and magnitude of the discharge jet. When compared with the

experiments, the discharge jet in simulation has smaller axial component. Since this component has been distributed in the other two velocity components, there is an observed change in direction and hence, a shift is observed in the location of maximum downward axial velocity. Disparityis also observed in the near wall values of axial velocity which are supposedly to be approaching zero for the final data points at 137 mm and 142 mm radius. The experimental values are unable to reflect it, while CFD simulations are able to provide realistic results in this zone. In the regions lower than quarter of the tank radius, difference in axial velocity is also observed.. This disparity might be due to less data points in this region. A detailed scrutiny of the flow field shown in figure 4 for this region reveals zone of very low axial velocities and clockwise circulation around it. Decreasing axial velocities in this region can also be observed in the figures showing flow field of solid phase given in the same paper (Guida et al., 2010).
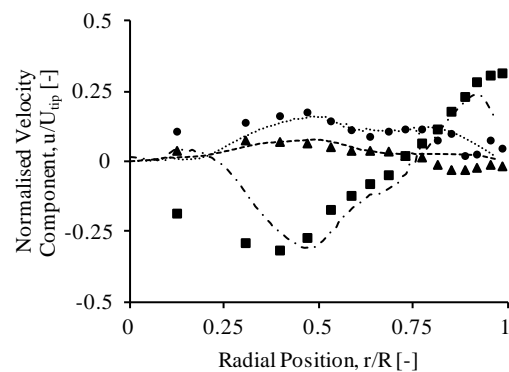
Figure 2: The three velocity components in a horizontal plane at z/H = 0.2 for 20 wt% and N=N$_{js}$. ■ Experimental Axial Velocity ▬ ∙ ▬ ∙ Simulated Axial Velocity ▲ Experimental Radial Velocity ▬ ▬ Simulated Radial Velocity ● Experimental Tangential Velocity ∙∙∙∙∙∙∙∙ Simulated Tangential Velocity
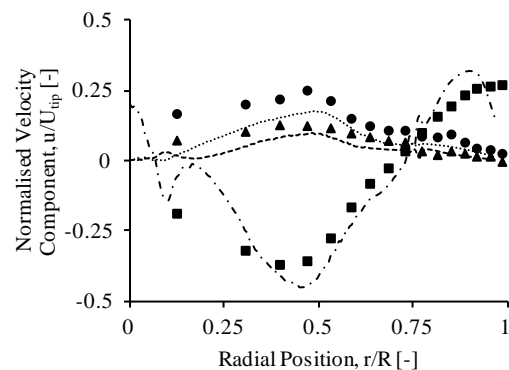
Figure 3: The three velocity components in a horizontal plane at z/H = 0.2 for 40 wt% and N=Njs. ■ Experimental Axial Velocity ▬ ∙ ▬ ∙ Simulated Axial Velocity ▲ Experimental Radial Velocity ▬ ▬ Simulated Radial Velocity ● Experimental Tangential Velocity ∙∙∙∙∙∙∙∙ Simulated Tangential Velocity

Once satisfactory results were obtained for 20% solids loading, the model was applied for a higher solid concentration of 40 wt %. The comparison with the experimental data is shown in figure 3. While the simulation results matched well qualitatively with the experimental data, the simulations predicted lower radial and tangential velocities. However, it should be noted that

the RMS error in the difference in value is 0.08 and is not significant as compared to the normalised velocity values. At this solids loading, distribution of axial component of velocity in other two components was not observed. This is probably due to the differences in the turbulence and turbulence dissipation predicted at such a high volume fraction of solids. It resulted in an over-prediction of drag as the drag is derived from the local values of ε. The effect on the turbulence is discussed in later part of the paper. In the experimental results, the local solids concentration near the impeller was found to be lower for 40 wt% solids case and therefore, the effect of reduction in velocity components was not that prominent as in the case of 20 wt% solids. The increase in solid concentration should have dampened the turbulence and therefore, the drag exerted on particle (Ochieng & Onyango, 2008; Wadnerkar et al., 2012). However, the prediction of accurate level of turbulence dampening is still erratic in the impeller region (Derksen, 2003). Although, the simulations were able to predict the higher velocity components due to lower local solid concentration but in the present case, lower dissipation and higher turbulence values might have resulted in further increased values of velocity components.

From the above discussion, it is clear that the modified Brucato drag model can be successfully applied to higher solids concentration and particle Reynolds numbers. With this assertion, other parameters were analysed for the performance analysis of stirred tank.

Flow Field and Velocity Components

The flow field generated by the PBTD for single phase and the two concentrations viz. 20% and 40% by wt are shown in figure 4. For the PBTD, a downward discharge jet is formed which is inclined radially outwards. The jet approaches the bottom of the tank and moves radially outwards towards the wall. The high velocity of the jet encounters the bottom and side wall of the vessel and then moves upwards forming a loop. The magnitude of velocity was high in the impeller region and in the flow loop, but low velocity was observed in the centre of loop and the upper parts of the tank. Similar behaviour was observed with the studies that used axial impellers for the investigations (Bittorf & Kresta, 2003; Guida et al., 2010). In the presence of particles, a significant reduction in the jet velocity is observed due to dampening of turbulence models (Wadnerkar et al., 2012) (see Figure 4(b) and 4(c)). A detailed examination shows a change in the flow structure. A shift in the centre of the flow loop can be observed from single phase to multiphase. The centre of loop has shifted axially upwards and radially inwards. Guida et al. (Guida et al., 2010) also observed similar phenomenon. The shift in the centre of loop is a result of the change in the direction of discharge jet well before hitting the bottom wall. On analyzing the presence of solids near the bottom wall, a high concentration zone of solid was observed. The high concentration of solid offered a low-clearance to the impeller generated flow and imposed resistance to the flow loop. Such a phenomenon has been observed by Kasat et al.(Kasat et al., 2008) and Sardeshpande et al. (Sardeshpande, M. V., 2009) for radial flow impellers and termed it as "false-bottom effect". This is also the reason of decreasing solid velocities in the vicinity of bottom of the tank with the increase in solid concentration.

The radial, axial and tangential velocities of solid particles at impeller discharge plane for 20 wt% and 40 wt% solids

are shown in Figure 2 and Figure 3 respectively. The comparison shows the axial velocity as the dominant component out of the three as is expected for the PBTD. The axial velocity follow the trend shown in Figure 4. It reaches a maximum when the discharge flow passes through the plane. Therefore, the maximum axial velocity (negative) was found to around 0.46 of r/R. Moving radially outwards, the axial velocity gradually approaches zero and advances towards positive values due to the upward flow of the loop near the walls.

The positive axial velocities near the centre of the tank are visible in the plots of Figure 2 and Figure 3. These positive values are a result of clockwise secondary loop observed in the low radius regions below the impeller (Figure 4(b) and 4(c)). The experiments in the paper by Guida et al. (Guida et al., 2010) were not able to capture it due to less number of data points. But, the similar behaviour has been captured and reported in few other studies (Pianko-Oprych et al., 2009). The radial and tangential velocity component are comparatively small. These components are found to be significant only in the impeller discharge region and tend to diminish when moving away from this field.

Interestingly, when comparing the axial velocity components for cases of 20 wt% and 40 wt% solids, the magnitude was higher for 40 wt% of solids. On detailed scrutiny, it was observed that the "false bottom effect" became more dominant in this case resulting in a lower concentration of solids in the impeller zone. Also, due to this reason, a further inclination of the jet was also observed in Figure 4. Therefore, the net decrease in the velocity in this particular region for 40 wt% solid is lesser than the dampening for 20wt% solid. As a result velocity in the discharge stream of 40wt % solids is higher than that for 20 wt% solids.

(a)　　　　(b)　　　　(c)
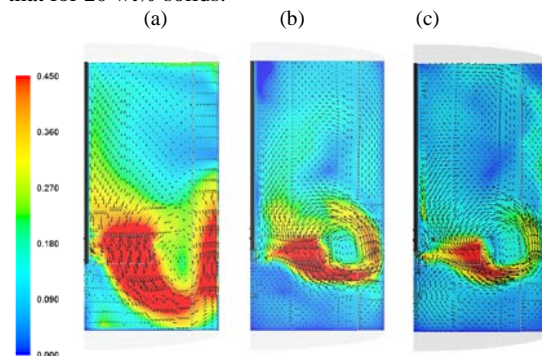
Figure 4: Normalised velocity maps and velocity vectors at mid-baffle plane for N = N_{js} of(a) single phase, (b) solid phase (20 wt%) and (c) solid phase (40 wt%).

Slip Velocity

The slip velocities were calculated using the time averaged component of velocity of the two phases and is shown in Figure 5. The slip velocities were normalised using impeller tip velocity. The relaxation time for the particles has a very high value of 1.2425 and the Stokes number was 9.94 and 12.21 for 20wt% and 40 wt% cases respectively. These values are indicator of presence of high slip velocities in the stirred tank. The high values of slip velocities were found in the impeller discharge region, vicinity of the side wall and near the impeller rod. The high values in the impeller discharge are expected due to the force exerted to the fluid accelerates it strongly but the particles acceleration is low due to the inertia. This supports the finding of Ljungqvist et al. (Ljungqvist &

Rasmuson, 2004). High slip velocities near the side wall and impeller rod are mainly due to combination of the effect of gravity and inertial forces. In the near wall region, high slip velocities located above the impeller plane are due to particles lagging the flow. In this region, the fluid flow is decelerating and due to a very high Stokes number the particles detach from the flow. For the near wall region below the impeller plane, the fluid leads and then lags the particle with the decreasing axial position. In the region of the loop where high fluid velocities encounter the wall, the fluid leads the solid. But below the loop, the fluid velocity approaches zero and the particles tend to settle down due to the absence of enough drag and presence of gravity, hence leaving the fluid behind. With careful examination, it can be observed that when the velocity vectors are pointing downwards (towards gravity), the particles tend to gain velocity and lead the flow and when the velocity is in opposite direction of the force of gravity, particle lag behind due to inertia and fluid lead the flow. This effect was also noticed and reported in literature (Ljungqvist & Rasmuson, 2001; Ochieng & Onyango, 2008; Pianko-Oprych et al., 2009). Similar effect can also be observed in the near impeller region and in the clockwise secondary loop below the impeller.
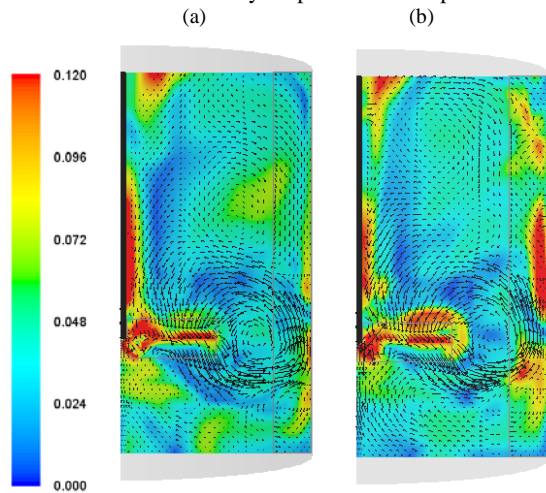
Figure 5: Normalised slip velocity maps and velocity vectors at mid-baffle plane for $N = N_{js}$ of (a) 20 wt% solid and (b) 40 wt% solids.

The dampening of the turbulence due to the increased solid concentration might be a possible reason for it. The drag model used in the simulation takes into account the turbulence effect at Kolmogorov length scale (Wadnerkar et al., 2012). Therefore, the simulations proved helpful in analysing the dampening of turbulence with increasing solid concentration. Its effect was noticed while comparing the slip velocity contours for the two cases. Due to this dampening, magnitude of slip velocity increased with the increase in concentration.

Turbulent Kinetic Energy

Normalised values of turbulent kinetic energy (TKE) was calculated by dividing the turbulent kinetic energy by the square of the tip velocity for the comparison of three cases. The simulation result show very high value of kinetic energy in the impeller swept region (Figure 6(a)). Since the value of TKE in the bulk was several order of magnitude lower than that in the impeller region, therefore log scale was used for the colormap to show the change in even smaller values of TKE in the domain. Since the plane

cuts the impeller blade, the magnitudes of TKE ahead of the impeller blade and that behind the impeller blade are also visible. The flow ahead of the impeller blade possess atleast double the TKE as that which follows the blade. The TKE is found to decrease with the advance of the flow loop and decreases by an order of magnitudes as the loop approaches wall. The difference in the TKE of the loop and the bulk is atleast two order of magnitude.

In order to understand the effect on turbulence due to presence of solids, the comparison with the single phase is necessary. The direction of flow loop changedin the presence of solids resulting in the observed drastic dissimilarity in the contours of TKE with and without solids. The high values followed the loop and were also observed in the upper portion of tank rather than bottom as was seen in single phase flow. The acute change of several order of magnitudes in the TKE in flow loop region is due to the simultaneous presence of high concentration of particles flowing along the loop. From Figure 6, the dampening of the turbulence and the increase in the dampening with the increase in particle concentration is evident. The same characteristic was also pointed out by studies in literature (Bittorf & Kresta, 2003; Guida et al., 2010). The turbulent structure provides energy to disperse the high concentration of solid particles, but at the same time the solid particles may result in the dampening of the turbulence (Barresi & Baldi, 1987; Bittorf & Kresta, 2003). Only when the particle size is sufficiently close to the eddy length microscale, the particle behavior was unaffected by external turbulence. The eddy–particle interaction was reasoned as the basic mechanism for solids distribution in a stirred liquid (Pinelli et al., 2004).The settling velocity changes in the stirred tank in the conditions where the particle diameter is comparable to the Kolmogoroff microscale and eddies have significant influence on particle motion (Magelli et al., 1990). For $dp/\lambda>10$, the interaction between energy dissipating eddies and particles become important for the solids concentration distribution (Ochieng & Onyango, 2008). For the cases studied in the paper, the average value of this ratio was far higher than 10.
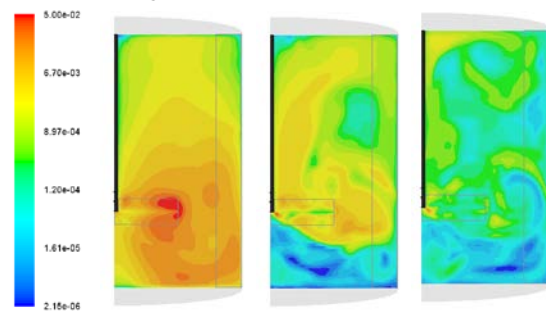
Figure 6: Normalised turbulent kinetic energy contours at mid-baffle plane for $N = N_{js}$ of (a) single phase, (b) solid phase (20 wt%) and (c) solid phase (40 wt%).

Power Number

The power number is a global criterion providing an estimate for the power dispersed in mixing by an impeller. It is given as:

$$N_P = \frac{P}{\rho_m N^3 D_i^5}$$

The power delivered to the fluid can be derived by multiplying the torque delivered to the fluid with the impeller speed, $2\pi N$. The torque (M) is obtained by

integration of the pressure on the impeller blade. Therefore the power is given by:

$$P = 2\pi NM$$

For the cases discussed, the increase in the power number with the increase in solids concentration was observed. Bubbico et al. (1998) performed experiments for investigation of effects of large particles suspension on the agitation power. They also observed the increase in the power number with the increase in concentration and accredited it to the increased drag in the case of large particles. However, the results obtained in the cases simulated in the paper donot show a linear increase in the power number as is shown by Bubbico et al. (1998). The power number increases from 1.67 for single phase to 2.11 for 20 wt% solids and 2.34 for 40 wt% solids. The rate of increase of the power dissipated decreased with increase in concentration reduces as the Euler-Euler simulations are not able to include the energy lost due to the particle collisions. Therefore, considering a linear increase in the solid concentration, it can be concluded that the power requirement increase considerably for the better suspension in the stirred tank.

CONCLUSION

CFD simulations were conducted for simulating stirred tanks with high solid concentration. The effect of high solid loading on the performance of stirred tank was conducted by the analysis of flow field, velocity components, slip velocity, turbulence kinetic energy and power number. The conclusions of the study are summarised below:

1. Modified Brucato drag model worked well upto the particle concentration of 20wt% and Reynolds number of 1.91×10^5. The predictions of the drag model deviated while predicting the velocity components of cases with higher solid concentration (40 wt%) due to underprediction of drag. A careful application of drag model is recommended for the high concentration of solids in stirred tanks.

2. The increased solid concentration substantially changed the flow field. The 'false bottom effect' at very high solid concentration results in higher velocity values compared to moderate solid concentration cases.

3. High slip velocity were found below the impeller, near the wall and near the impeller rod for PBTD. The magnitude of slip velocities increased due to increase in solid concentration.

4. Dampening of turbulence was dominant due to the presence of particles. At higher concentration, significant power is required to counteract the dampening and for the dispersion of solids.

5. The power number linearly increases with the increase in concentration. External forces need to be accommodated to incorporate the effect of energy dissipation due to particle collision at high solid concentration.

REFERENCES

ANSYS, (2009), "Fluent User Guide". from ANSYS Inc.: Canonsburg, PA, www. fluent. com

BARIGOU, M., (2004), "Particle Tracking in Opaque Mixing Systems: An Overview of the Capabilities of PET and PEPT", *Chem. Eng. Res. Des.,* **82(9),** 1258-1267.

BARRESI, A., & BALDI, G., (1987), "Solid dispersion in an agitated vessel", *Chem. Eng. Sci.,* **42(12),** 2949-2956. doi: Doi: 10.1016/0009-2509(87)87060-4

BITTORF, K. J., & KRESTA, S. M., (2003), "Prediction of Cloud Height for Solid Suspensions in Stirred Tanks", *Chem. Eng. Res. Des.,* **81(5),** 568-577.

BUBBICO, R., et al., (1998), "Agitation power for solid-liquid suspensions containing large particles", *The Canadian Journal of Chemical Engineering,* **76(3),** 428-432. doi: 10.1002/cjce.5450760312

CHAOUKI, J., et al., (1997), "Noninvasive tomographic and velocimetric monitoring of multiphase flows", *Industrial & engineering chemistry research,* **36(11),** 4476-4503.

DERKSEN, J. J., (2003), "Numerical simulation of solids suspension in a stirred tank", *American Institute of Chemical Engineers. AIChE Journal,* **49(11),** 2700-2700.

FRADETTE, L., et al., (2007), "CFD phenomenological model of solid-liquid mixing in stirred vessels", *Computers & Chemical Engineering,* **31(4),** 334-345.

GUIDA, A., et al., (2010), "PEPT measurements of solid-liquid flow field and spatial phase distribution in concentrated monodisperse stirred suspensions", *Chem. Eng. Sci.,* **65(6),** 1905-1914.

KASAT, G. R., et al., (2008), "CFD simulation of liquid-phase mixing in solid-liquid stirred reactor", *Chem. Eng. Sci.,* **63(15),** 3877-3885. doi: DOI: 10.1016/j.ces.2008.04.018

KHOPKAR, A. R., et al., (2006), "Computational Fluid Dynamics Simulation of the Solid Suspension in a Stirred Slurry Reactor", *Industrial & Engineering Chemistry Research,* **45(12),** 4416-4428. doi: 10.1021/ie050941q

LJUNGQVIST, M., & RASMUSON, A., (2001), "Numerical Simulation of the Two-Phase Flow in an Axially Stirred Vessel", *Chem. Eng. Res. Des.,* **79(5),** 533-546.

LJUNGQVIST, M., & RASMUSON, A., (2004), "The Two-Phase Flow in an Axially Stirred Vessel Investigated Using Phase-Doppler Anemometry", *The Canadian Journal of Chemical Engineering,* **82(2),** 275-288.

MAGELLI, F., et al., (1990), "Solid distribution in vessels stirred with multiple impellers", *Chem. Eng. Sci.,* **45(3),** 615-625. doi: Doi: 10.1016/0009-2509(90)87005-d

MONTANTE, G., & MAGELLI, F., (2005), "Modelling of solids distribution in stirred tanks: analysis of simulation strategies and comparison with experimental data", *International journal of computational fluid dynamics,* **19(3),** 253-253.

OCHIENG, A., & LEWIS, A. E., (2006), "CFD simulation of solids off-bottom suspension and cloud height", *Hydrometallurgy,* **82(1-2),** 1-12.

OCHIENG, A., & ONYANGO, M. S., (2008), "Drag models, solids concentration and velocity distribution in a stirred tank", *Powder Technol.,* **181(1),** 1-8.

PIANKO-OPRYCH, P., et al., (2009), "Positron emission particle tracking (PEPT) compared to particle image velocimetry (PIV) for studying the flow generated by a pitched-blade turbine in single phase and multi-phase systems", *Chem. Eng. Sci.,* **64(23),** 4955-4968.

PINELLI, D., et al., (2004), "Dispersion coefficients and settling velocities of solids in slurry vessels stirred with different types of multiple impellers", *Chem. Eng. Sci.,* **59(15),** 3081-3089.

RASTEIRO, M. G., et al., (1994), "Modelling slurry mixing tanks", *Adv. Powder Technol.,* **5(1),** 1-14. doi: Doi: 10.1016/s0921-8831(08)60620-2

SARDESHPANDE, M. V., (2009), "Solid Suspension and Liquid Phase Mixing in Solid-Liquid Stirred Tanks", *Industrial & Engineering Chemistry Research,* **48(21),** 9713-9713.

SARDESHPANDE, M. V., et al., (2009), "Solid Suspension and Liquid Phase Mixing in Solid-Liquid Stirred Tanks", *Industrial & engineering chemistry research,* **48(21),** 9713-9713.

STEVENSON, R., et al., (2010), "Analysis of partial suspension in stirred mixing cells using both MRI and ERT", *Chem. Eng. Sci.,* **65(4),** 1385-1393.

UNADKAT, H., et al., (2009), "Application of fluorescent PIV and digital image analysis to measure turbulence properties of solid-liquid stirred suspensions", *Chem. Eng. Res. Des.,* **87(4),** 573-586.

WADNERKAR, D., et al., (2012), "CFD simulation of solid–liquid stirred tanks", *Adv. Powder Technol.* **(0)**. doi: 10.1016/j.apt.2012.03.007

YAMAZAKI, H., et al., (1986), "Concentration profiles of solids suspended in a stirred tank", *Powder Technol.,* **48(3),** 205-216.